CENTRIFUGAL ACCELERATION OF IONS IN THE POLAR MAGNETOSPHERE

by

Kenneth R. Swinney

and

James L. Horwitz

Department of Physics

The University of Alabama at Huntsville

Huntsville, Al. 35899

D. Delcourt

Space Sciences Laboratory

NASA/ Marshall Space Flight Center

Huntsville, Al. 35812

Submitted to:

Journal Geophysical Research

March 1987

Abstract

The transport of ionospheric ions originating near the dayside cusp into the magnetotail is parametrically studied using a 3-D model of ion trajectories. It is shown that the 'centrifugal' term in the guiding center parallel force equation dominates the parallel motion after about 4 Re geocentric distance. The dependence of the equatorial crossing distance on initial latitude, energy and the convection electric field is presented for ions originating on the dayside ionosphere in the noon-midnight plane. It is also found that up to altitudes of about 5 Re, the motion is similar to that of a bead on a rotating rod, for which a simple analytic solution exists.

1. Introduction

It is currently accepted that the ionosphere is an important source of magnetospheric plasma [e. g. , Horwitz, 1982]. Plasma of ionospheric origin has been observed throughout the magnetosphere. Observations over the polar cap have suggested that the dayside cleft is a source of ionosphereic ions [Shelley et al., 1982, Waite et al., 1985; Lockwood, et al., 1985; Moore et al., 1984; Peterson, 1985]. Ionospheric ions have also been observed in the plasma sheet [e.g. Sharp, 1982; Lennartsson et al., 1985; Stockholm et al., 1985] and the plasma lobes and mantle [Hardy et al., 1977; Frank et al., 1977; Sharp et al., 1981; Candidi et al., 1982]. In order to understand the properties of ionospheric ions in the magnetosphere several researchers have developed models to calculate the trajectories of ions originating in the ionosphere. Horwitz [1984] and Horwitz and Lockwood [1985] used a 2-D model to calculate trajectories and distribution functions of ions originating near the dayside cleft in the noon-midnight plane. Cladis and Francis [1985] used a 3-D model to calculate the transport of ions from the plasma sheet to the ring current. More recently Cladis [1986] used the same model to study parallel acceleration of ions from the polar ionosphere to the plasma sheet. Sauvaud and Delcourt [1987] used a 3-D model to study suprathermal ionospheric ion trajectories.

In his paper, Cladis [1986] established that the centrifugal acceleration causes low energy ions (with just enough energy to overcome gravity) originating near the dayside cusp to be accelerated to several keV at the point where they cross the

magnetospheric equator. To help understand the properties (e. g. location and energy) of ionospheric ions entering the plasma sheet, we present calculations that give the initial conditions for which an ionospheric ion will cross the equator at a particular distance in the tail. These calculations were made as part of a parametric study of properties of ionospheric ion transport in the magnetosphere.

2. Model

The trajectory calculation is started by specifying the initial position (as radius, latitude and local time (0^{o} at noon)), mass, energy, and pitch angle of the ion. The three dimensional trajectories are then determined using the guiding center approximation. The motion of the guiding center parallel to the magnetic field is found by integrating the guiding center parallel force equation [Northrup,1963]

$$\dot{v}_{\parallel} = \vec{g} \cdot \hat{b} + \frac{e}{m} \vec{E} \cdot \hat{b} - \frac{\mu}{m} (\vec{\nabla} B) \cdot \hat{b} + \vec{v}_D \cdot \frac{d\hat{b}}{dt} \qquad (1)$$

where $v_{\parallel}$ is the velocity in the direction of the magnetic field, $\vec{g}$ is the gravitaional acceleration, m is the mass of the ion, and e its charge, μ is the first adiabatic invariant, B and $\hat{b}$ are the magnitude and direction of the magnetic field, and $\vec{v}_D$ is the guiding center drift velocity. The last term on the right is the centrifugal force. It is the fictitious force that must be included due to the angular acceleration of the particles reference frame. This can be seen most clearly for a radial magneitc field (a monopole source) for which case the term in

question becomes $\omega r \frac{d\hat{r}}{dt}$, which is the centrifugal force with angular speed $\omega = V_{Do}/r_o$ (V_{Do} is the drift velocity at the injection radius r_o).

The motion of the ion perpendicular to the magnetic field is calculated using the guiding center perpendicular drift velocity [Northrup, 1963]

$$\vec{V}_D = \vec{V}_e + \vec{V}_g + \vec{V}_{\nabla B} + \hat{b} \times \frac{mc}{e} \frac{d}{dt} \vec{V}_e \qquad (2)$$

where $\vec{V}_e$ is the drift due to the convection electric field, $\vec{V}_g$ is the gravitational drift and $\vec{V}_{\nabla B}$ is the drift due to gradient and curvature of the magnetic field. The first adiabatic moment is conserved by adjusting the gyration velocity after each time increment.

The convection electric field at a point on the trajectory is determined using the Heelis et al [1982] model for the convection electrostatic potential of the high-latitude ionosphere. The Heelis et al model is an analytic expression for the potential, envolving 14 parameters. The total potential is expressed as the product

$$V(\theta, \bar{\varphi}) = G(\theta)\ F(\theta, \bar{\varphi}) \qquad (3)$$

where θ is the colatitude, and $\bar{\varphi}$ is the azimuthal angle defined to be zero at noon. The function $G(\theta)$ models the strongest colatitude dependence of the potential. The potential goes through a minimum at the flow reversal boundary , the location of which is colatitude T_o. Equatorward of the convection reversal boudary , the potential is modeled as by Volland , the parameter r_1 describing the exponent by which the potential decreases. Poleward the potential increases in a similar fashion with r_2 the

exponent , and a phase angle T_c included to allow for non-zero flow velocities over the pole. The convection reversal boudary is given a width , T_1 and T_2, either side of T_o , inside of which the functional form of G is choosen to keep the flow velocity (or electric field) continuous across the boundary. The function F models the local time dependence of the potential, by allowing the zero potential line to be at local times ξ_d (dayside) and ξ_n (nightside). The angular widths of the convergence zones at the reversal boundary are specified by the parameters ξ_d^+ and ξ_d^- for the dayside and a similar pair for the night side. The widths are modified by a latitude dependence that gives the narrowest width at colatitude T_o, and 90^o at the pole. The magnitude of the potential is specified by the potentials , V_m and V_e, of the morning and evening reversal boundaries, respectively. All the trajectories calculated in this study (unless specific values are specified otherwise) used a set of parameters that give a uniform field of 56.7 mV/m over the pole with this model and they are: $T_o = 73^o$, $T_1 = 72^o$, $T_2 = 74^o$, $\xi_d = 0^o \pm 90^o$, $\xi_n = 180^o \pm 90^o$, and $V_m = -V_e = 106.3$ kVolts. The magnitude of the convection electric field is varied by changing the magnitude of V_m. To calculate the convection eletric field at a particular point, our approach is to trace the magnetic field from the point of interest in the magnetosphere to its conjugate point in the ionosphere, where the electrostatic potential is determined using the Heelis model(assuming the magnetic field lines are equipotentials). The potential of two points near the point of interest are also determined, and the electric field is then calculated.

3. Parametric Studies

3.1 Effect of centrifugal acceleration on low altitude ions

Earlier two dimensional studies by Horwitz [1984] of ionospheric ions originating near the dayside cusp did not include the centrifugal term in the parallel force equation. For low energy ions the contribution of the centrifugal term to the parallel energy can become significant at 3 to 4 Re geocentric distance. This is demonstrated in figure (1) for a 12 eV O^+ ion, where the total energy is plotted against geocentric distance for trajectories calculated with and without the centrifugal force term. The curves begin to separate near 3 Re. At a given altitude a particle will have had less time to drift perpendicular to $\vec{B}$ when the centrifugal term is included, therefore the calculated trajectories are significantly different if the ion rises significantly above the point where the energy curves separate.

3.2 Comparison to earlier studies

Cladis [1986] pointed out that ionospheric ions originating near the dayside cusp gain several keV of energy as they move into the magnetospheric tail because the changing magnetic field direction the particle sees along its trajectory causes the particle to drift across electric equipotentials. This centrifugal acceleration term in the parallel force equation can be thought of as being due to either the ion encountering a changing magnetic field direction or a perpendicular drift velocity which is changing in the direction of the magnetic field. These two veiws are equivalent since $\frac{d}{dt}(\vec{V}_D \cdot \hat{b})$ is zero.

In order to compare the results of our calculations to those presented by Cladis [1986], trajectories were calculated using the same injection parameters. The parameters for the Heelis model were chosen to give a uniform convection electric field over the polar cap. Figure (2a) shows four trajectories for ionospheric convection electric fields (over the pole at 1.05 Re) 23.3, 40, 56.7 and 80 mV/m. Figure (2b) depicts the total energies as a function of flight time. These results are presented for comparison with Cladis [1986], and are in general agreement. The shape of the energy curve is similar but the final energies are not as large as those published by Cladis [1986]. The differences can be accounted for by the different magnetic field models used to make the calculations. A qualitative comparison between the two field models shows that ring current contribution taken into account in the model used by Cladis leads to less curved field lines outside the equatorial plane and more curvature very near the euqatorial plane. As a result, at high latitudes, a particle will gain energy sooner in the Luhman-Friesen field model. Near the equator the larger curvature in the model used by Cladis will cause the particle to experience a stronger curvature drift, almost perpendicular to the local equipotentials, resulting in a larger gain in parallel energy.

The total kinetic energy and the parallel and perpendicular components for trajectory 2 from figure (2a) are plotted against time of flight in figure (2c) and against geocentric distance in figure (2d). These figures show that the major contribution to the kinetic energy is the parallel component. The convection

kinetic energy is significant but smaller than the parallel kinetic energy. It is the perpendicular drift across equipotentails (out of the noon-midnight plane) that allows the particle to gain energy. However, the net drift is small (less than 1 Re at the equator) and is not plotted here.

3.3 A physical analogy

It has been demonstrated in the above sections that by 4-5 Re the centrifugal term dominates the parallel motion for ions that can overcome gravity. For much of such a particle's trajectory the only significant contribution to acceleration comes from the last term in equation (1). Another physical system, whose motion is dominated by centrifugal force, is a bead on a rigid, frictionless rod rotating with a constant angular velocity, ω . The motion is determined by the centrifugal force and the trajectory can be found by solving

$$\ddot{r} = \omega^2 r \qquad (4)$$

If the bead is injected at time zero at radial distance r_0, angle θ_0 and velocity V_0, the solutions for r and θ as functions of time are

$$r = r_0 \cosh(\omega t) + (V_0/\omega) \sinh(\omega t)$$
$$\theta = \omega t + \theta_0 \qquad (5)$$

The velocity at time t is

$$\vec{V} = \dot{r}\,\hat{r} + r\,\omega\,\hat{\theta}$$
$$\dot{r} = \omega\,(r_0 \sinh(\omega t) + (V_0/\omega) \cosh(\omega t)) \qquad (6)$$

The distance at which the bead crosses the negative x-axis ($\theta = \pi$) if it is injected above the positive x-axis is determined by the injection point and the ratio V_0/ω. If we designate r_c as the crossing distance and t_c as the crossing time, then

$$t_c = (\pi - \theta_0) / \omega$$
$$r_c = r_0 \cosh(\pi - \theta_0) + V_0/\omega \sinh(\pi - \theta_0) \quad (7)$$

Thus, for a particular injection location, the crossing distance is determined by the ratio of V_0/ω. The velocity at crossing depends on the above ratio and the value of ω. Thus beads injected at the same point with V_0/ω constant will cross the x-axis at the same distance with different energies.

The similarity between the bead on the rod and an ion originating in the ionosphere near the dayside cusp arises because the motion of each is dominated by the centrifugal term in the respective force equations. In its reference frame the ion sees moving magnetic field lines which constrain its motion in much the same way that the rod constrains the motion of the bead. The analogy is not exact because the magnetic field lines are not straight, but as figure (3) indicates, the trajectories of the bead and the ion agree reasonably if ωr is taken as being analogous to the perpendicular guiding center drift velocity. Figure (3a) shows the trajectories of 2 ions injected at the same location (r=1.2 Re, $\lambda=70^o$, noon) with different energies (12 and 20 eV). The trajectories of beads on a rod are also shown for the same location and injection parameters. Figure (3b) shows ions and beads injected with same energies (12 eV) and different locations (r=1.2Re, $\lambda=70^o$ and 80^o, noon). The point where the bead trajectory crosses the ion trajectory increases as the initial energy increases (for the same initial λ). A bead's trajectory more closely follows the ion's the more poleward the injection location (for the same

energy) because the magnetic field is more radial. However, the two trajectories cross at lower r when λ is larger. The analogy breaks down because as the ion moves radially outward, its angular speed is not constant. For a dipole magnetic field with a uniform westwardly convection elcetric field over the polar cap, the angular speed increases as $\sqrt{r}$.

3.4 Parametric study

The parametric study of the centrifugal acceleration was performed by varying the injection parameters over a wide range of values and examinig the equatorial crossing distance (x) and energy. A uniform convection eletric field of 56.7 mV/m was used in the following calculations unless otherwise specified. The study was further restricted to O^+ ions which were injected on the dayside at 1.2 Re altitude in the noon-midnight plane, except where other parameters are specified.

Trajectories were calculated for ten different injection latitudes, varying from 66^o to 84^o, with an injection energy of 12 eV and pitch angle (α) of 150^o. Figure (4) shows that the distance at which the ion crosses the equatorial plane decreases with increasing injection latitude. This is because a lower injection laitiude causes the ion to convect onto magnetic field lines that cross the equator further into the tail. Figure (4b) shows that the kinetic energy at equatorial crossing decreases with increasing injection latitude. The ions injected at lower latitudes have a longer flight time, thus more time to gain energy from the changing magnetic field direction.

Trajectories were calculated for different injection local times and constant injection latitude (73^o) and energy (12 eV).

Both energy and distance at equatorial crossing were relatively constant, as is shown in figures (5a) and (5b). Figure (5c) shows the trajectories viewed from 45^{o} latitude and 21 hrs. local time.

Trajectories were calculated for 10 different energies ranging form 10 to 100 eV. The other parameters were in agreement with those used to calculate figures (4), with an injection latitude of 73^{o}. Figures (6a) and (6b) show that the equatorial crossing distance and energy icreases with injection energy. Furthermore, the crossing energy increases with crossing distance. This is because a particle with higher initial energy will convect less off the original field line and thus cross further in the tail. The centrifugal term in equation (1) contains the term $(\vec{V} \cdot \vec{\nabla})\hat{b}$. The larger an ions energy when it enters the region in the tail where the spatial gradient of $\hat{b}$ is largest, the more parallel energy it will gain. Thus the larger an ion's initial energy the more parallel energy it can gain from the changing magnetic field direction.

Inspection of figures (4a), (4b), (6a) and (6b) indicate that there is a relationship between equatorial crossing distance and energy. When all parameters except one are held fixed, the value of the varied parameter which allows the trajectory to cross the equatorial plane furthest in the tail also has the largest crossing kinetic energy. Another relationship between crossing distance and energy was shown for the bead on the rod analogy, namely that if $\sqrt{K_0}$ / Ep are held constant, the crossing distance is constant for a given injection location. The kinetic

energy at equatorial crossing depends on the above ratio and ω^2. Figure (7a) is a plot of crossing distance versus initial energy for a set of trajectories chosen such that the above ratio is constant with the same value as trajectory 2 in figures (2). For comparison, the curve from figure (6b) is graphed on the same plot. This figure demonstrates that for initail energies above 8 eV the crossing distance is nearly constant when the ratio $\sqrt{K_0}/Ep$ is held constant. The reason for the discrepancy at lower energies is because gravity is important for these trajectories. Figure (7b) shows the equatorial crossing energy for the same trajectories.

A more convenient method for displaying the dependence of the equatorial crossing point on the injection latitude and energy is illustrated in figure (8). In this figure, the horizontal plane represents the initial latitude (x-axis) and initial energy (y-axis) all other parameters being constant. The height above the horizontal plane (z-axis) represents the equatorial crossing distance. The surface plotted is composed of calculated trajectories at the intersection of each curve. This figure bears out in a more general format, what was indicated by the earlier figures. The higher the injection latitude, for a constant energy, the more earthward (smaller x) a trajectory crosses the equatorial plane. There is a dramatic difference between how quickly x increases with injection energy at the lower latitudes than at high altitudes. As was pointed out earlier, this is because trajectories starting at lower latitudes can convect onto field lines that cross the equatorial plane much further into the tail, while ions originating more poleward

convect onto field lines that cross more earthward. However, for the later ions increased energy also means less time for convection. These two opposing tendencies give an x which increases with injection energy, but at a slower rate as we go toward the pole in injection latitude. The shape of the surface on the lower latitude side rises to the point where ions can no longer reach the equatorial plane because they a) convect onto essentially 'open' field lines, b) cannot convect polewad enough and the trajectory crosses the equator on the dayside. Thus, our surface should approach infinity with decreasing injection latitude , then reappear from negative infinity and decrease toward 0. This surface is for a uniform convection electric field of 56.7 mv/m. A larger elctric field would give a different surface that would be lower near the origin and higher at larger latitude and energy. The surfaces would cross at the x where $\sqrt{Ko}/Ep$ is the same.

A horizontal plane representing constant x cuts the surface in figure (8a) along the curve plotted in figure (9). This figure represents the relationship between injection latitude and energy that crosses the equator at 12 (x's) and 14(+'s) Re.

4. Conclusions

The results presented in this paper give the relationship between the injection parameters and the equatorial crossing distance and energies for ions injected on the dayside ionosphere at noon local time. Several general conclusions have been reached as a result of this study. The centrifugal term must be included for trajectories that rise above 3 Re in altitude. The bead on a rotating rod analogy is useful in understanding the general dependence of the trajectories. For ions originating near the cusp the expression for the trajectory given by equation (5) might be sufficient for some studies, even though it does not give the exact trajectory. The distance at which an ion injected near the dayside cusp crosses the equatorial plane depends primarily on the injection location and the ratio of the injection velocity to convection electric field. The energy for the above ion at equatorial crossing depends strongly on the injection energy and convection electric field. When a single parameter is varied, there is a general trend for the energy to be higher for the parameter which causes the ion to travel furthest into the tail.

Referances

Candidi, M., S. Orsini, and V. Formisano, The properties of ionospheric O^+ ions as observed in the magnetotail boundary layer and northern plasma lobe, J. Geophys. Res., 87, 9097, 1982.

Cladis, J. B. and W. E. Francis, The polar ionosphere as a source of the strom time ring current, J. Geophys. Res., 90, 3465, 1985.

Cladis, J. B., Parallel Acceleration and Transport of Ions from Polar Ionosphere to Plasma Sheet , Geophys. Res. Lett., 13, 893, 1986.

Hardy, D. A., J. W. Freeman, and H. K. Hills, Double-peaked ion spectra in the lobe plasma: Evidence for massive ions, J. Geophys. Res, 82, 5529, 1977.

Heelis, R. A., J. K. Lowell, and R. W. Spiro, A model of high-altitude ionospheric convection patterns , J. Geophys. Res., 87, 6339, 1982.

Horwitz, J. L., The ionosphere as a source for magnetospheric ions, J. Geophys. Res., 20, 929,1982.

Horwitz, J. L. , Features of ion trajectories in the polar magnetosphere, Geophys. Res. Lett., 11, 1111, 1984.

Lennartsson, W. , R. D. Sharp and R. D. Zwickl. Substorm effects on the plasma sheet ion composition on March 22, 1979 (CDWA 6), J. Geophys. Res., 90, 1243, 1985.

Lockwood, M., and J. E. Titheridge, Ionospheric origin of magneotspheric O^+ ions, Geophys. Res. Lett., 8, 381, 1981.

Luhman, J. G. and J. F. E. Friesen, A simple model of the magnetosphere, J. Geophys Res. , 84, 4405., 1979.

Moore, T. E., J. H. Waite, Jr., M. Lockwood, M. O. Chandler, C. R. Chappell, M. Sugiura, D. R. Weimer, and W. K. Peterson, Upwelling O^+ ions: A case study (abstract), Eos Trans. AGU, 65, 1056, 1984.

Northrup, T. G., The Adiabatic Motion of Charged Particles, Interscience Publishers, New York, 1963.

Peterson, W. K., Ion injection and acceleration in the polar cusp, in THe Polar Casp, edited by J. A. Holtet and A. Egeland, pp. 67-84, D. Reidel, Dordrecht, 1985.

Sauvaud, J. A. and D. Delcourt, A numerical study of suprathermal ion trajectories in 3D electric and magnetic field models, J. Geophys. Res, 91, 1987.

Sharp, R. D., D. L. Carr, W. K. Peterson, and E. G. Shelley, Ion Streams in the magnetotail, J. Geophys. Res, 86, 4639, 1981.

Shelley, E. G., W. K. Peterson, A. G. Ghielmetti, and J. Geiss, The polar ionosphere as a source of energetic magnetospheric plasma, Geophys. Res. Lett., 9, 941, 1982.

Waite, J. H., Jr., T. Nagai, J. F. E. Johnson, C. R. Chappell, J. L. Burch, T. L. Killeen, P. B. Hayes, G. R. Carignan, W. K. Peterson, and E. G. Shelley, Escape of suprathermal O^+ ions in the polar cap, J. Geophys. Res., 90, 1619,1985.

Figure Captions

Figure (1) The parallel energy versus geocentric distance was calculated for an O^+ ion injected at an altitude of 1.3 Re, a latitude of 73^o, noon local time, 150^o pitch angle and a 56.7 mV/m convection electric field over the pole. Curve 1 was calculated with the centrifugal term in the force equation and curve 2 was calculated without the term.

Figure (2) The trajectories for O^+ injected near the dayside cusp (at (1.3Re, 68^o, 0^o)) for four different uniform convection electric fields; 80. mV/m (curve 1), 56.7 mV/m (curve 2), 40 mV/m (curve 3) and 23.5 mV/m (curve 4). The ions were injected with 12 eV energy and 150^o pitch angle. Figure a shows the trajectories , with an asterisk plotted every 1000 seconds, and b shows the energies plotted against flight time. The general behavior agrees with Cladis [1986]. Figures c and d show the contributions of the parallel and drift energies to the total energy for trajectory 2.

Figure (3) The trajectories for O^+ ions injected with 180^o pitch angle and 56.7 mV/m electric field are plotted The trajectories of a bead on a rotating rod are also In figure (3a) the ions (solid) and beads (dotted) which were injected at (r=1.2 Re, $\lambda=70^o$, noon) with 12 and 20 eV of energy. In figure (3b) they were injected with 20 eV and at (r=1.2Re, $\lambda= 70^o$ and 80^o, noon).

Figure (4) Trajectories for O^+ ions were calculated for ten different latitudes, varying from 66^o to 84^o. The other parameters were held constant; injected at 1.3 Re and 0^o local time, 150^o pitch angle, 12 eV energy and 56.7 mV/m

convection electric field. Figure a shows that the distance at which the ion encounters the equatorial plane decreases with increasing injection latitude. Figure b shows that the total energy at equatorial crossing also decreases with increasing injection latitude.

Figure (5) Trajectories were calculated for 5 different injection local times; noon and 10 and 20 degrees east and west of noon. The other parameters were fixed in agreement with figure (4) , with an injection latitude of 73^{o}. Both energy (figure a) and crossing distance (figure b) were constant. Figure c shows three of the trajectories; noon and $+20^{o}$ and -20^{o}.

Figure (6) Trajectories were calculated for 10 different energies ranging from 10 to 100 eV, all other parameters being held fixed in agreement with figure (4) with an injection latitude of 73^{o}. Figures a and b show that the equatorial crossing distance and energy increase with injection energy.

Figure (7) Trajectories were calculated with injection energy and convection electric field varied so that the ratio $\sqrt{K_0}/Ep$ remains constant. Figure a depicts the crossing distance against the initial energy (x). For comparison the curve from figure (6a) (+) is also included. All other parameters were fixed in agreement with figure (4) , with 73^{o} injection latitude. Figure b depicts final energy plotted against initial energy.

Figure (8) Trajectories were plotted by varying both the injection latitude and energy. The injection latitude was

varied from 66^{o} to 86^{o} in steps of 4^{o}, while the injection energy was varied from 10 eV to 70 eV. The other parameters were in agreement with figure (4) with an injection latitude of 73^{o}. The hieght above the horizontal plane (z-axis) represents the equatorial crossing distance, in figure a.

Figure (9) A plane at constant x, cuts the surface in figure (8a) defining the curve in this figure. The curves for two different equatorial crossing distances , 12 (x) and 14 (+) Re are plotted.

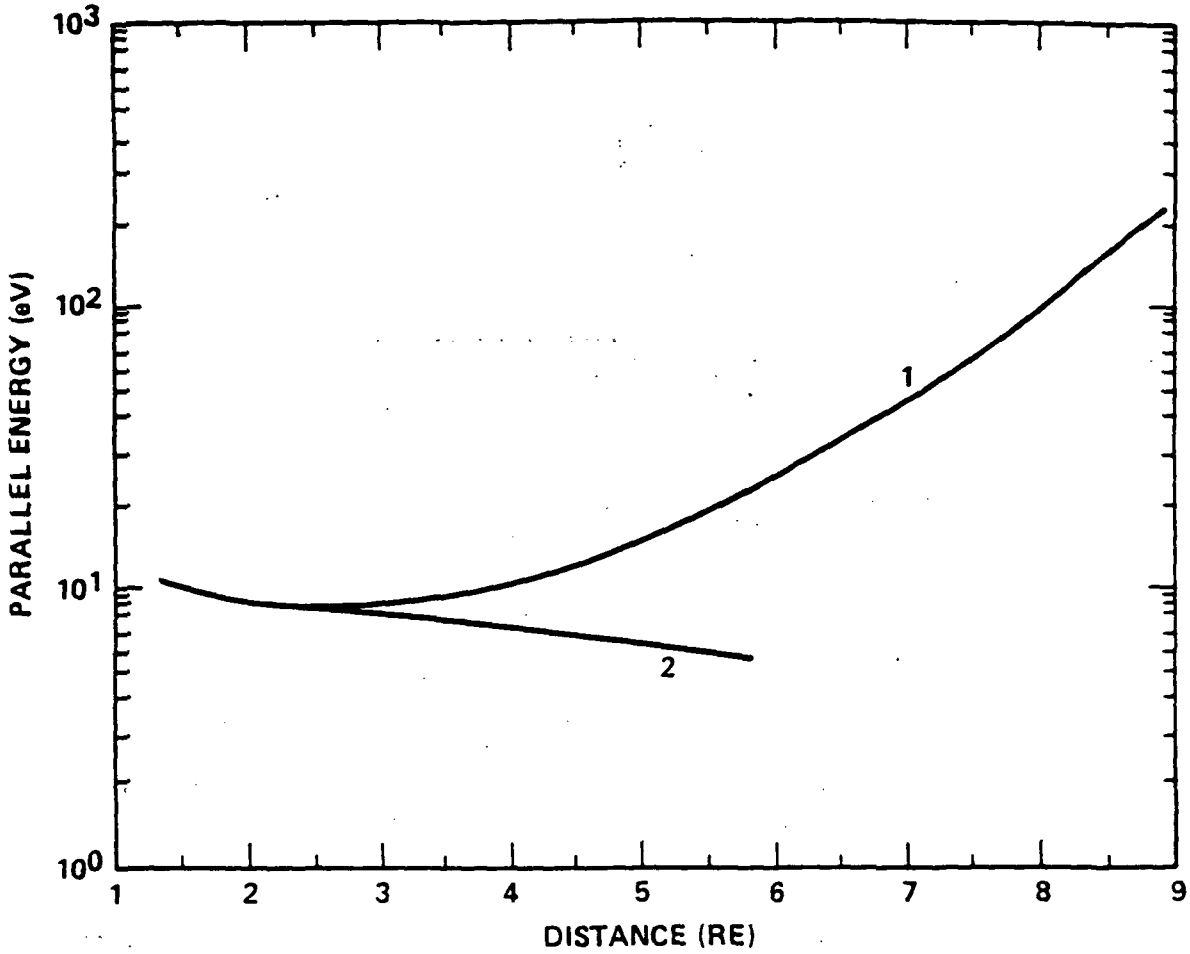

Figure (1)

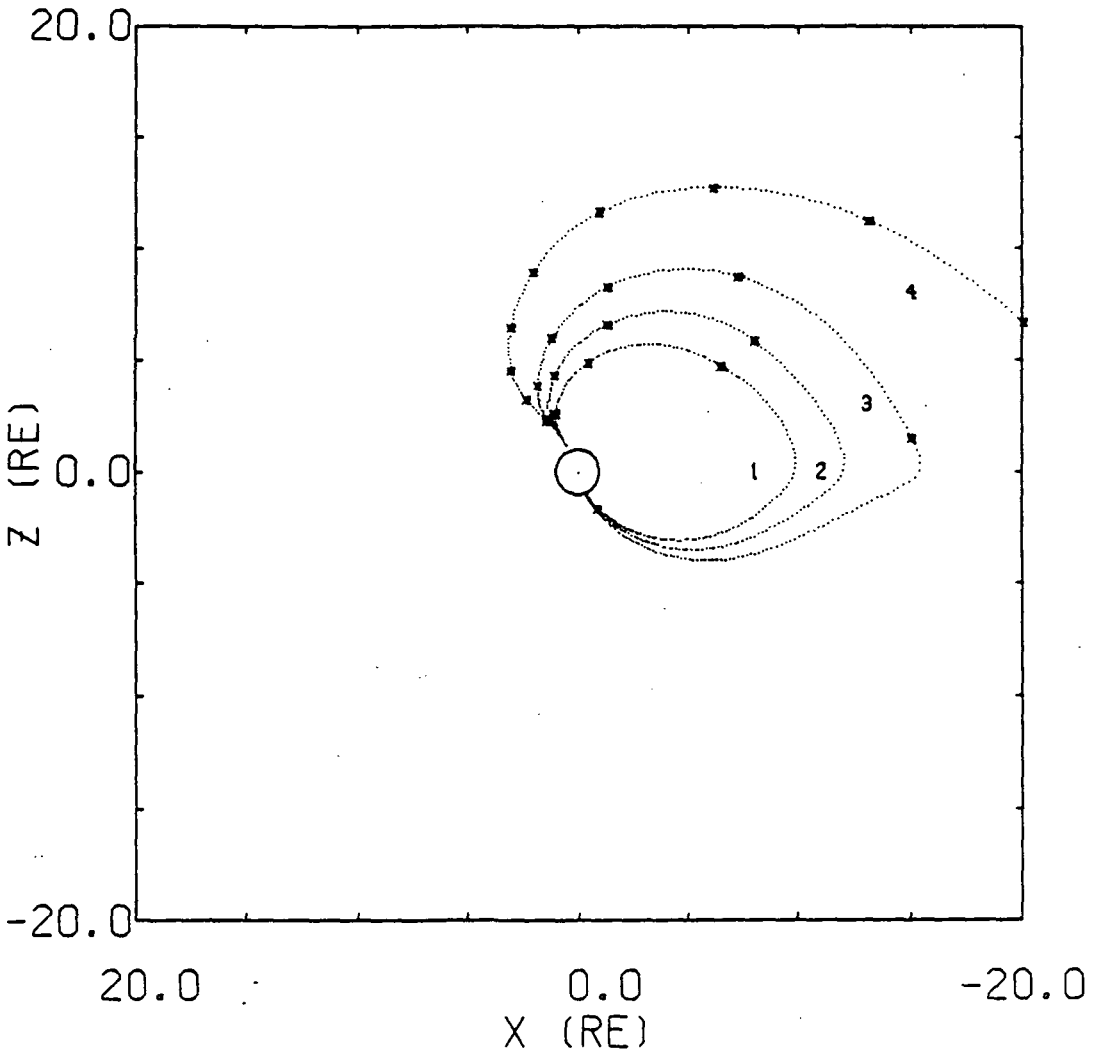

Figure (2a)

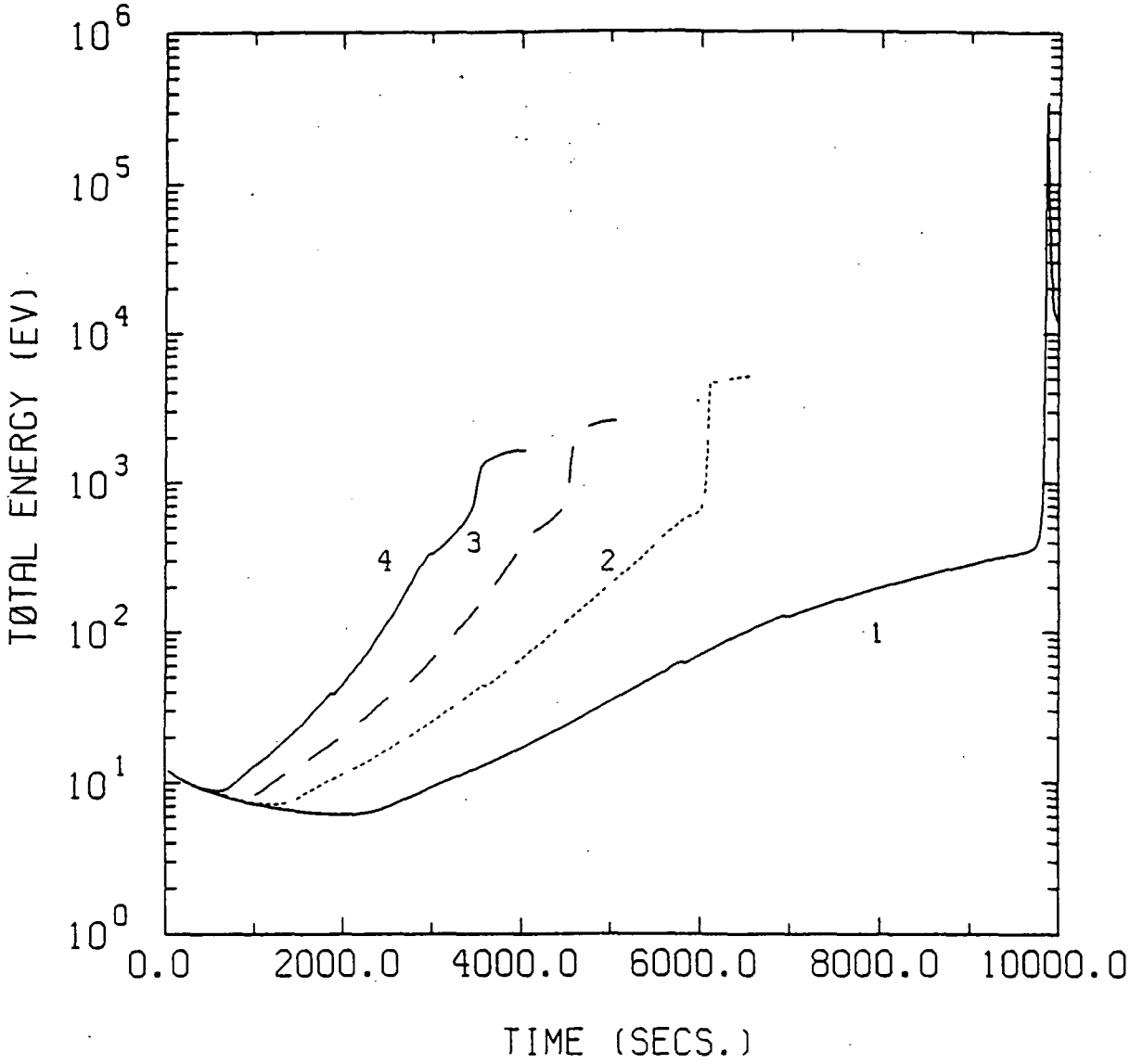
TØTAL ENERGY (EV)
10^6
10^5
10^4
10^3
10^2
10^1
10^0
0.0
2000.0
4000.0
6000.0
8000.0
10000.0
TIME (SECS.)
1
2
3
4

Figure (2b)

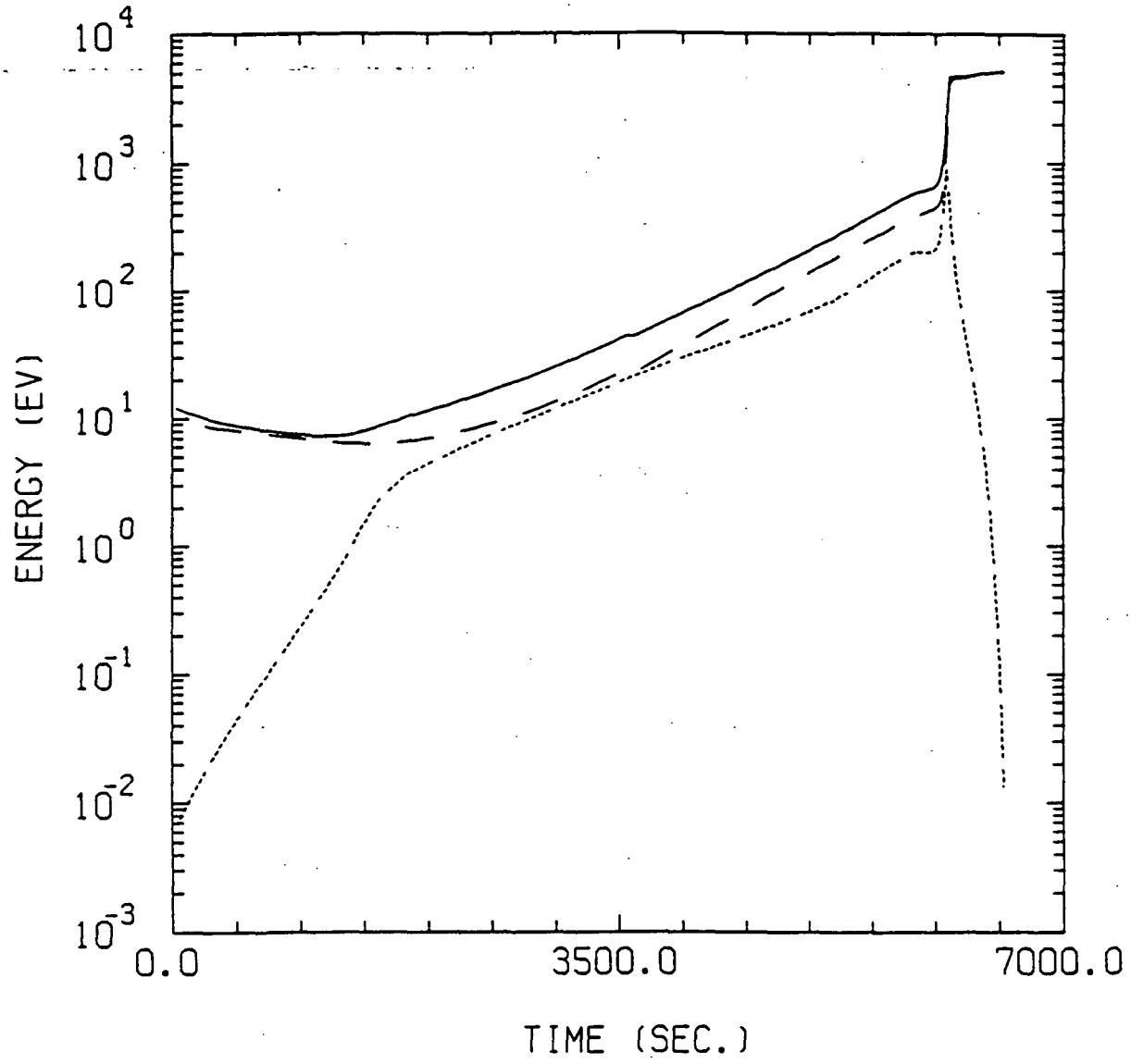
10^4
10^3
10^2
10^1
10^0
10^{-1}
10^{-2}
10^{-3}
ENERGY (EV)
0.0
3500.0
7000.0
TIME (SEC.)

Figure (2c)

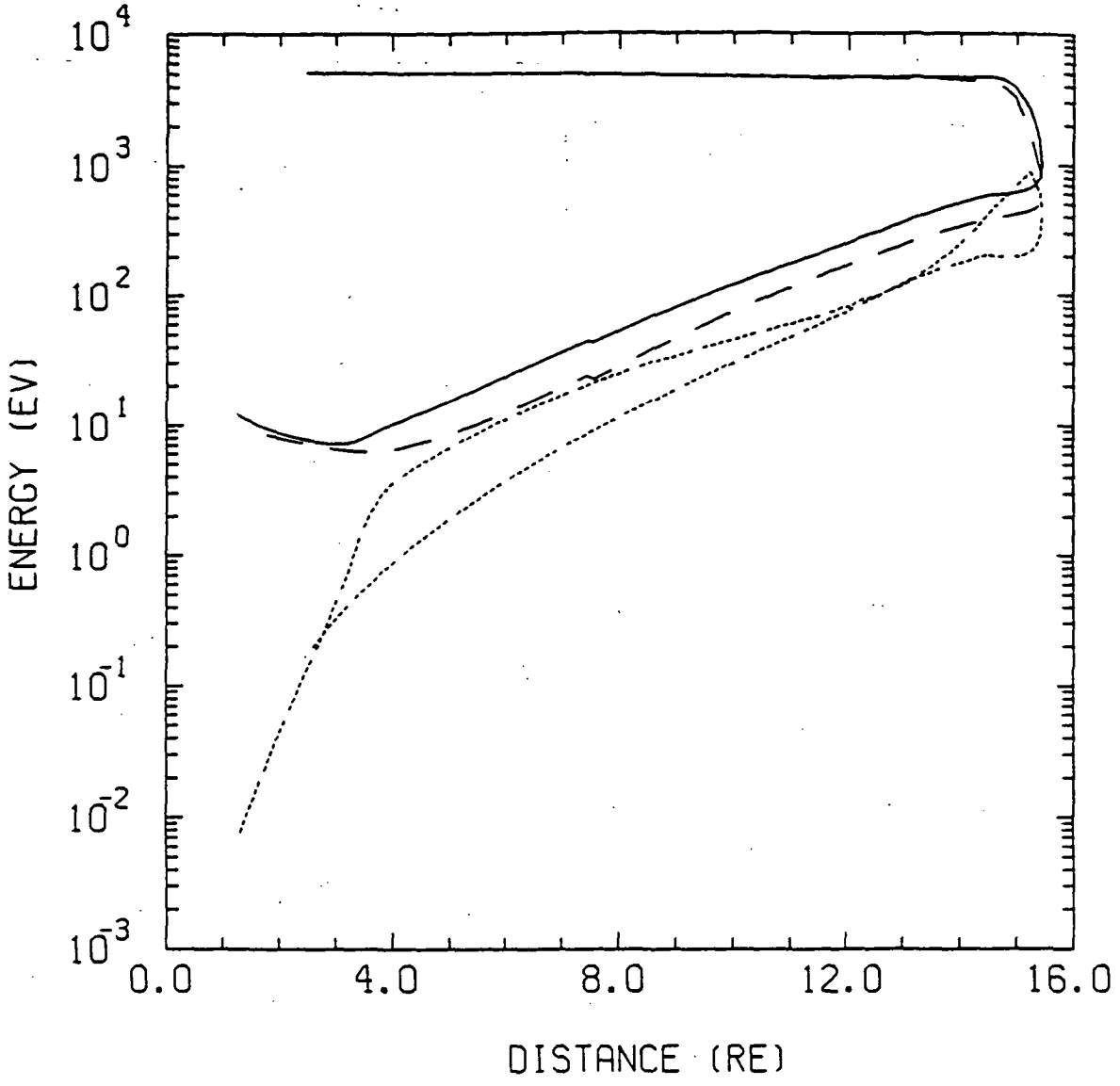
ENERGY (EV)
10^4
10^3
10^2
10^1
10^0
10^{-1}
10^{-2}
10^{-3}
0.0
4.0
8.0
12.0
16.0
DISTANCE (RE)

Figure (2d)

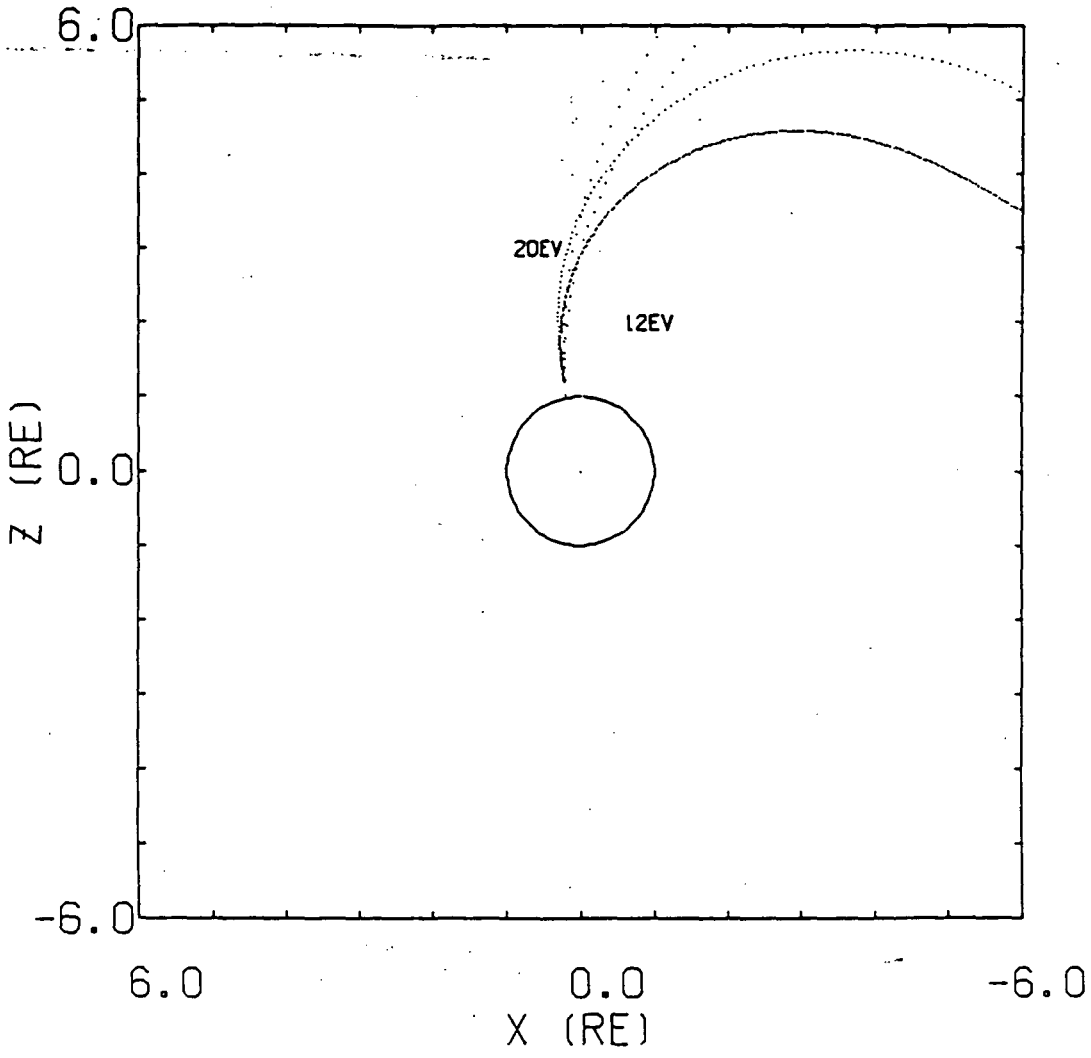

Figure (3a)

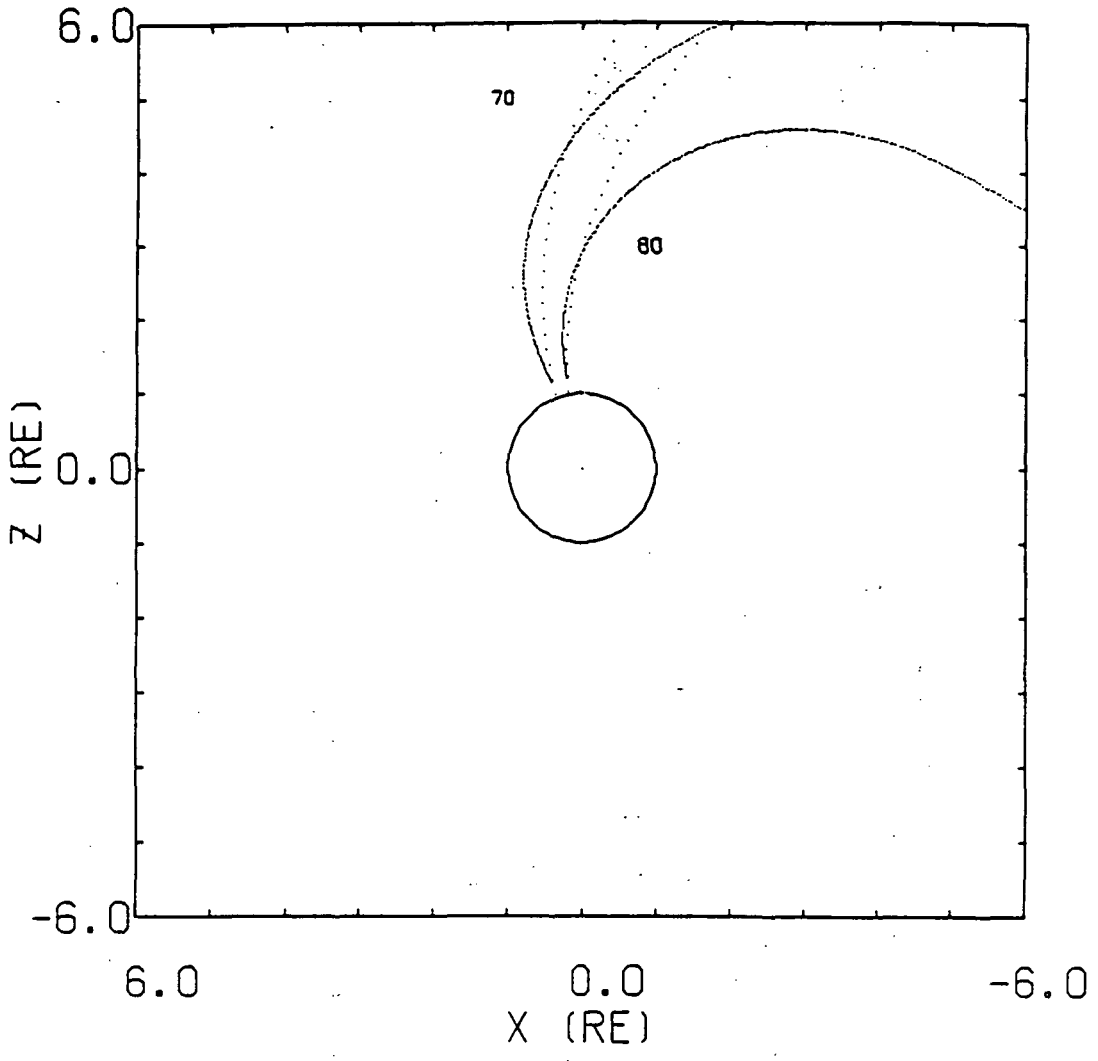

Figure (3b)

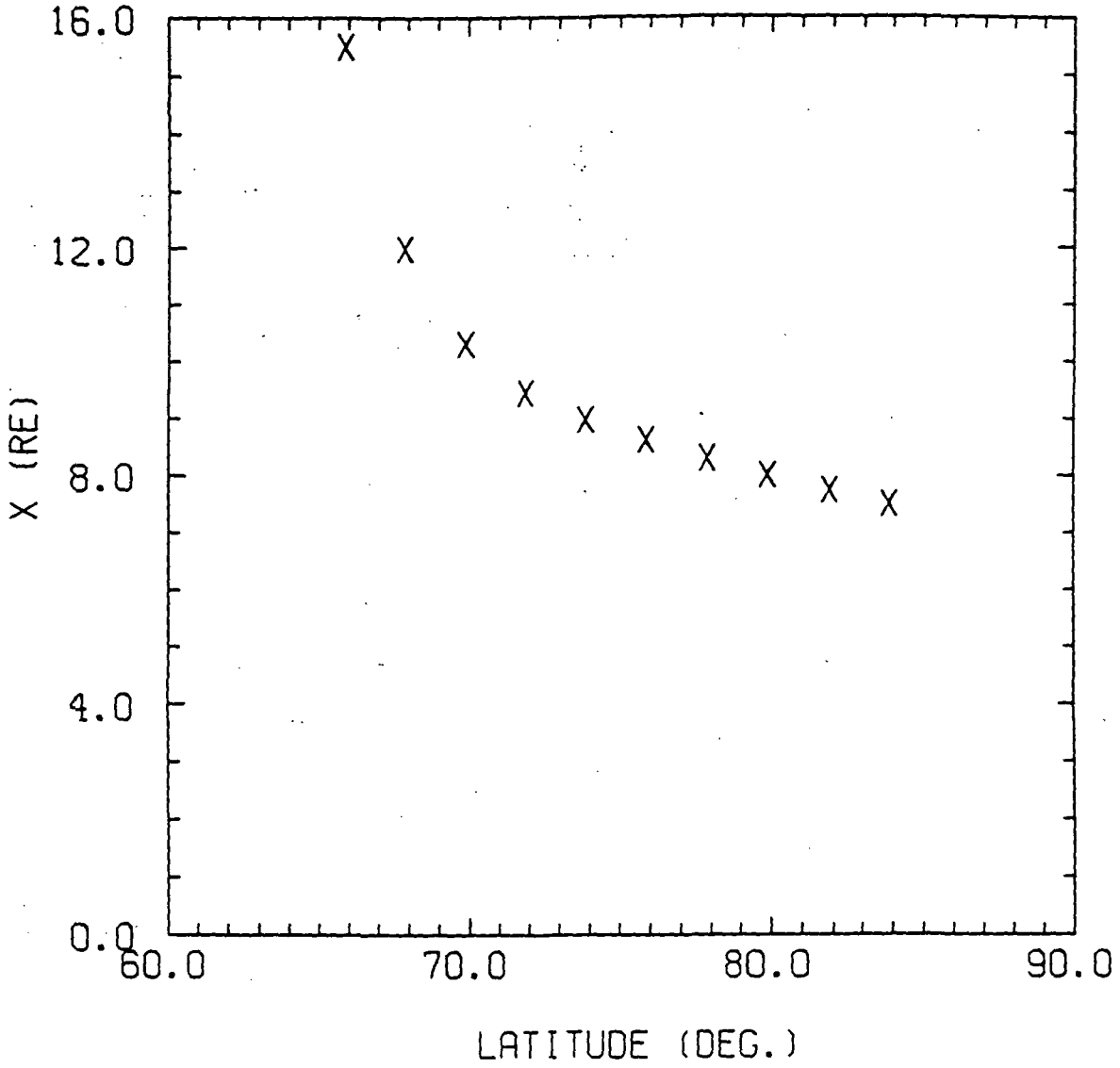

Figure (4a)

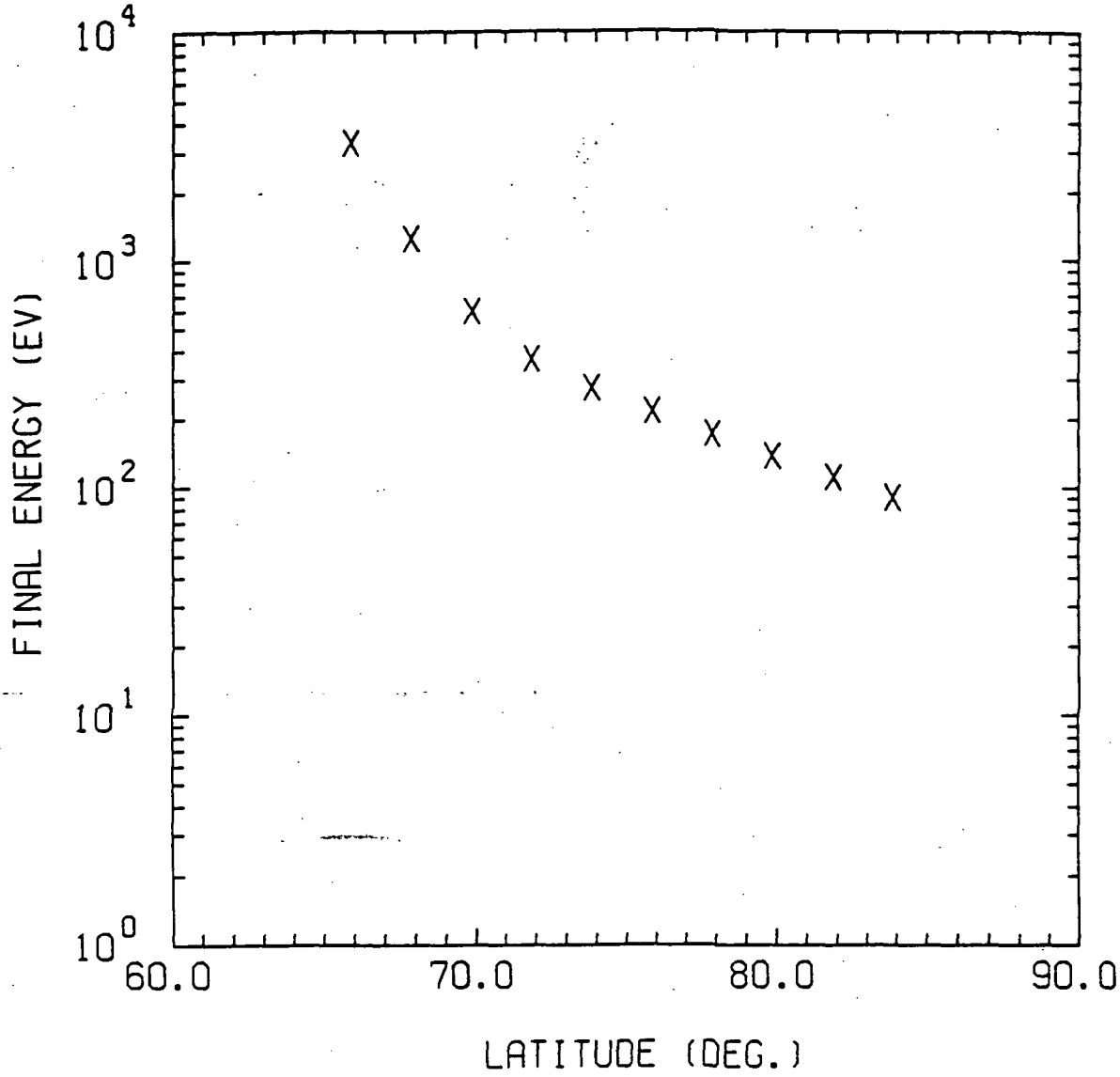
10^4
10^3
10^2
10^1
10^0
FINAL ENERGY (EV)
60.0
70.0
80.0
90.0
LATITUDE (DEG.)

Fifure (4b)

a

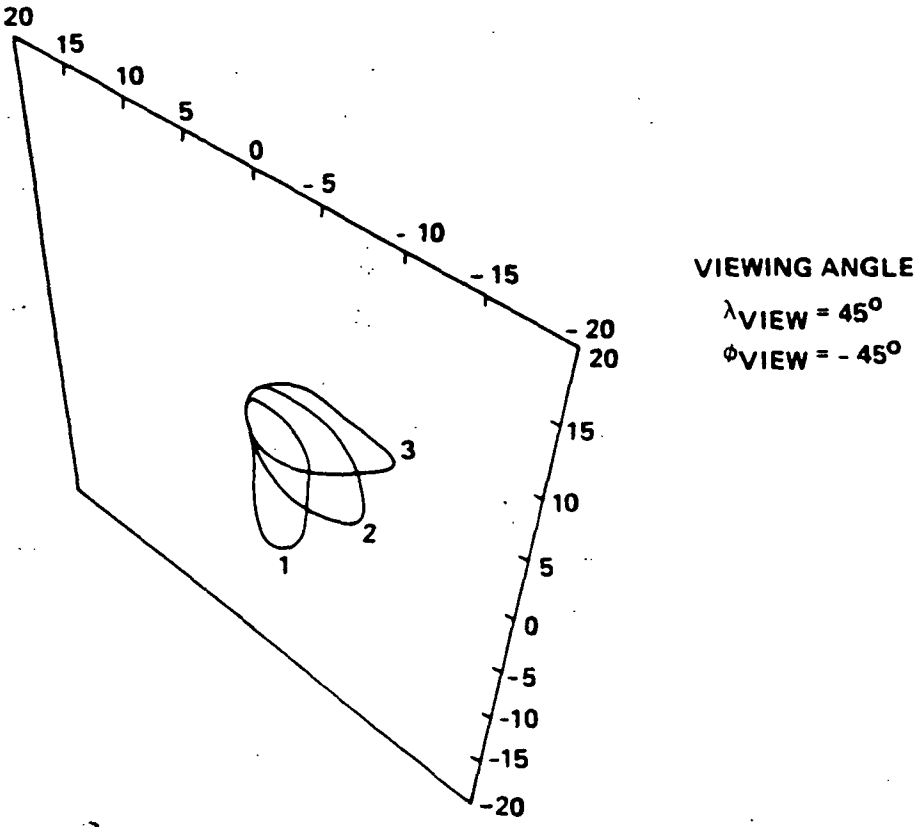
20
15
10
5
0
-5
-10
-15
-20
20
15
10
5
0
-5
-10
-15
-20
1
2
3
VIEWING ANGLE
λVIEW = 45°
ΦVIEW = - 45°

b

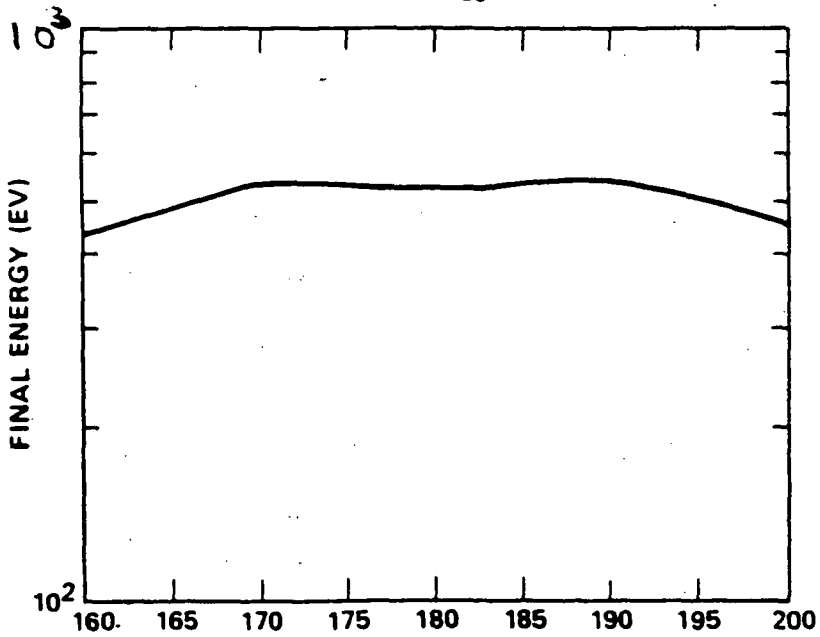
FINAL ENERGY (EV)
10²
160
165
170
175
180
185
190
195
200

Figure(5)

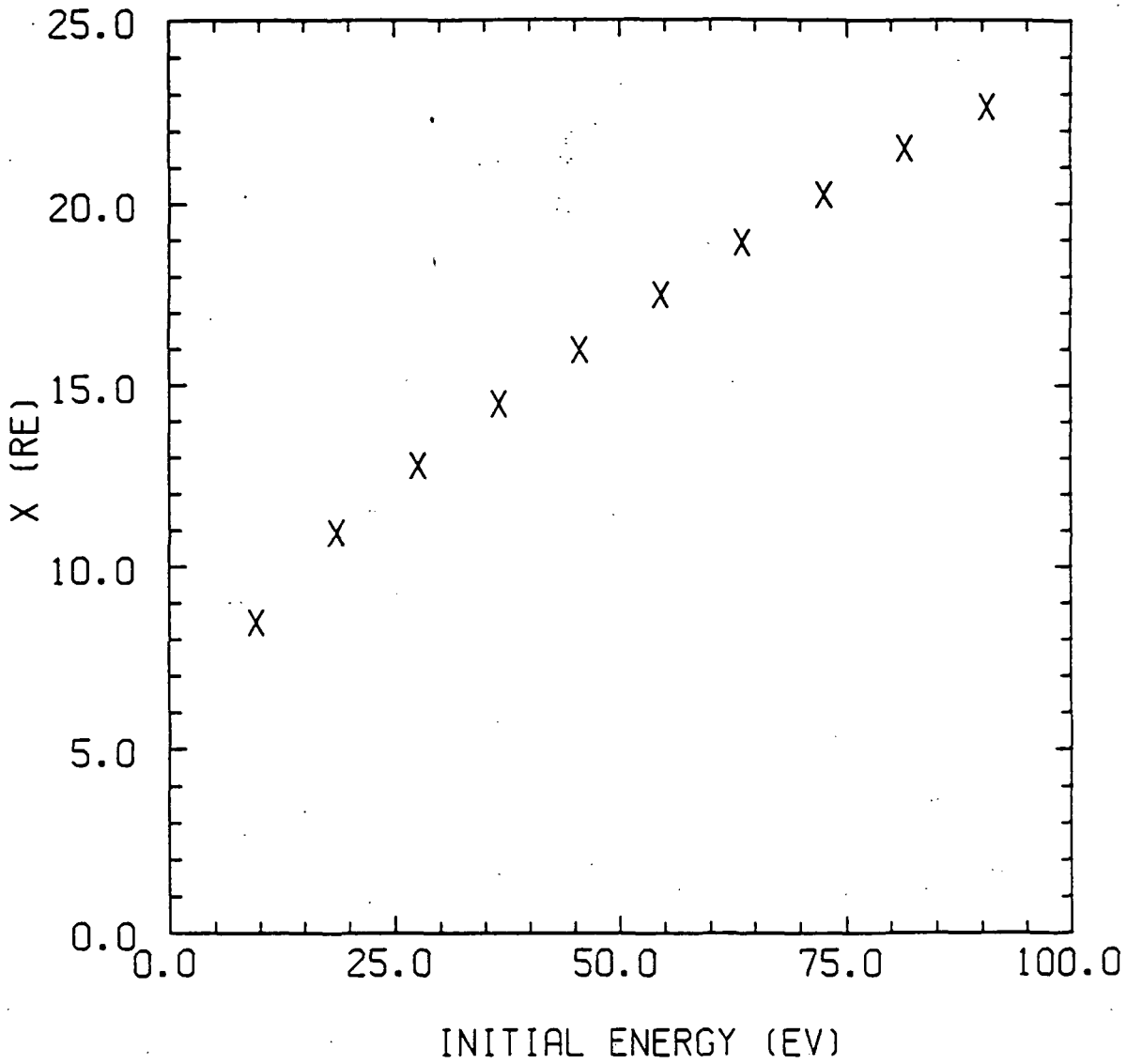

Figure (6a)

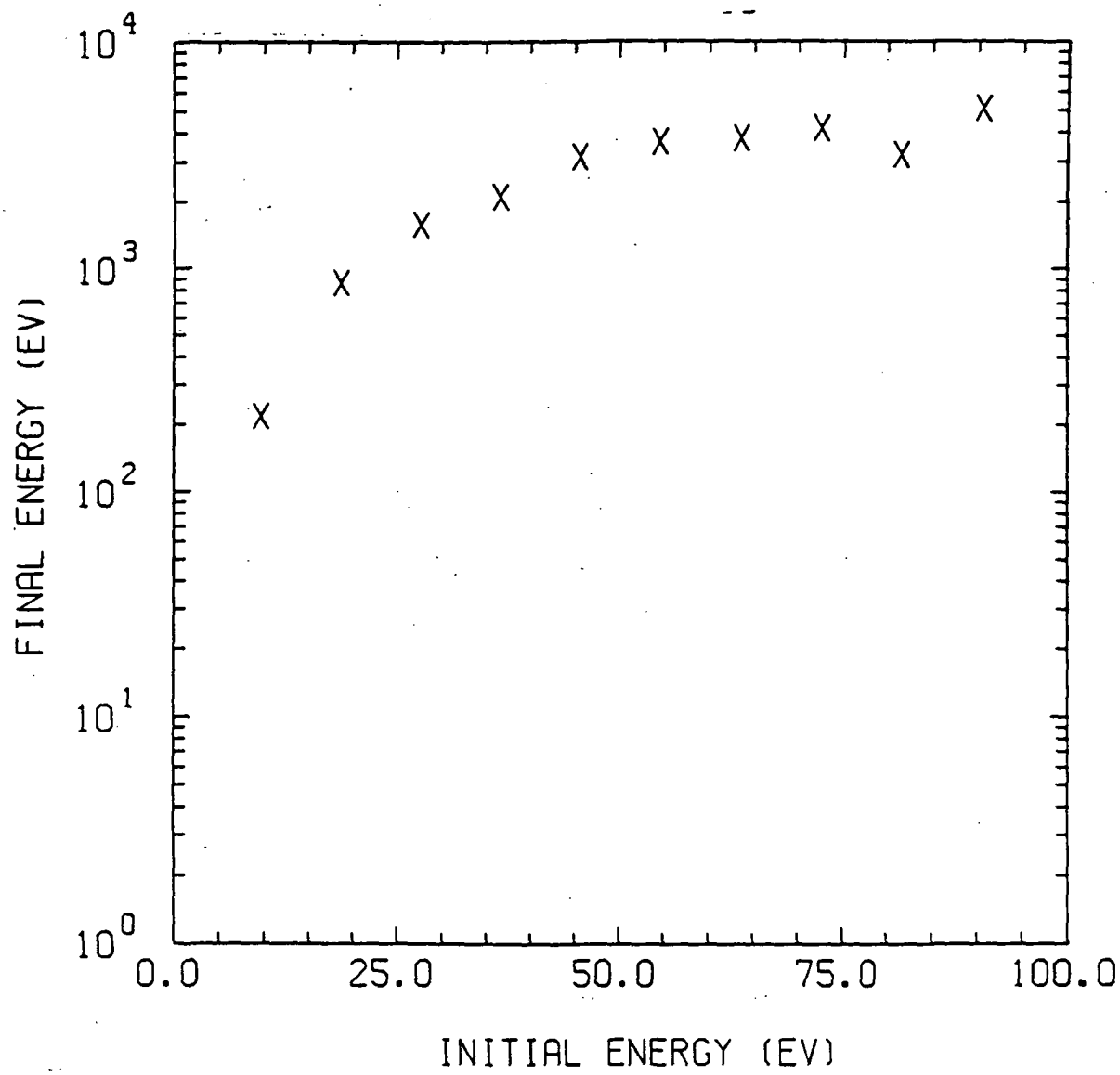
10^4
10^3
10^2
10^1
10^0
FINAL ENERGY (EV)
0.0
25.0
50.0
75.0
100.0
INITIAL ENERGY (EV)

Figure (6b)

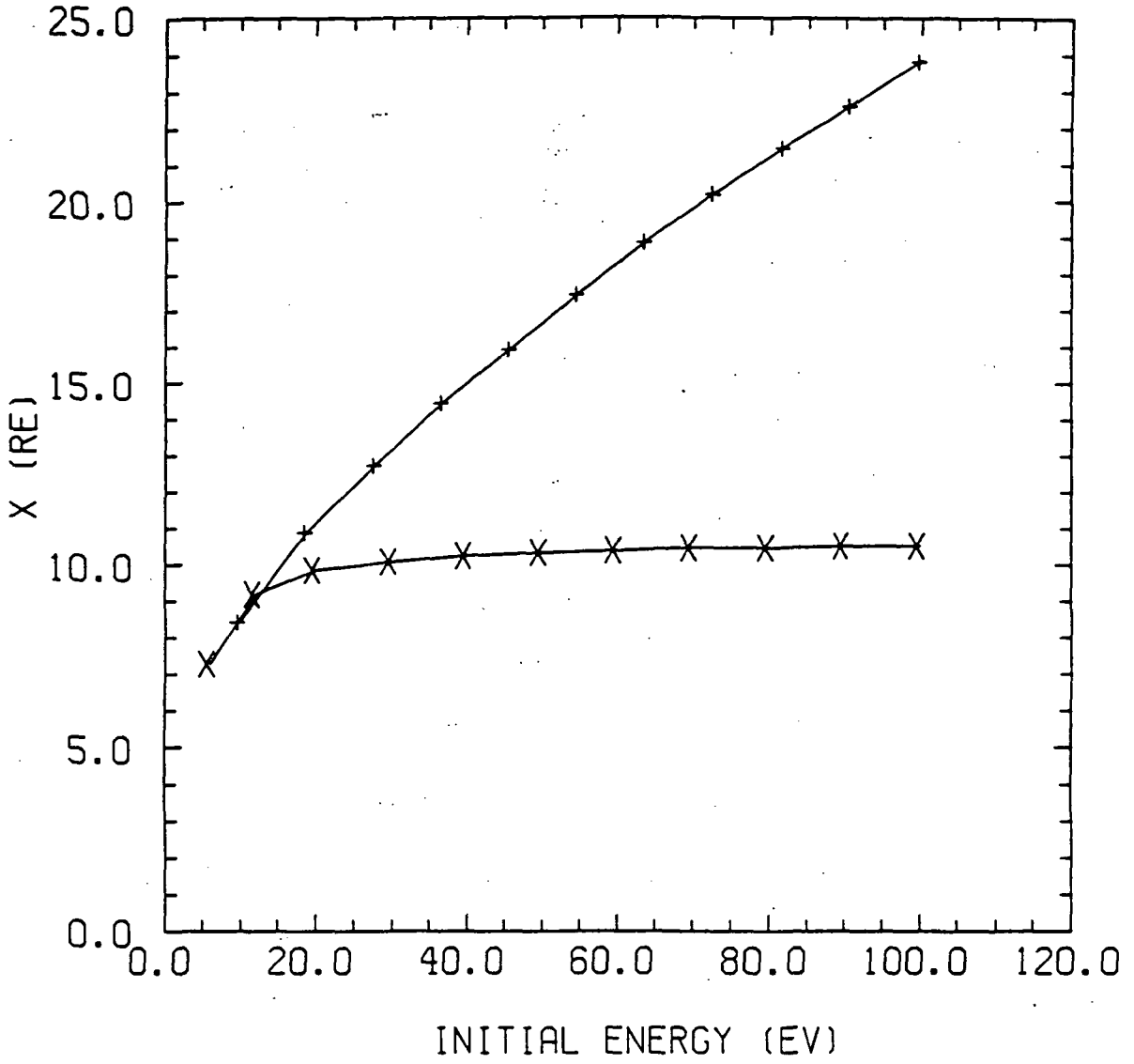
25.0
20.0
15.0
10.0
5.0
0.0
X (RE)
0.0
20.0
40.0
60.0
80.0
100.0
120.0
INITIAL ENERGY (EV)

Figure (7a)

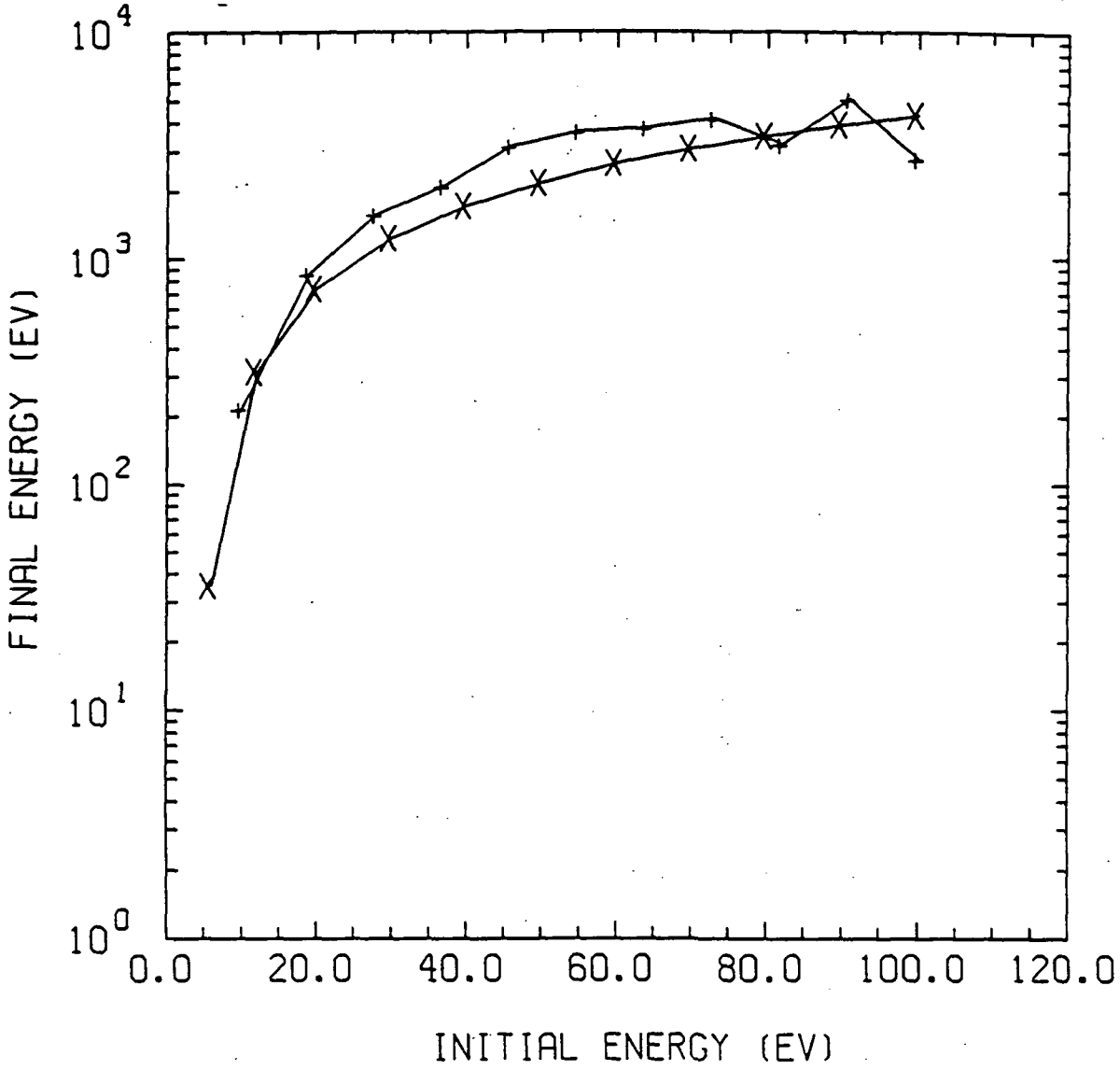
FINAL ENERGY (EV)
10^4
10^3
10^2
10^1
10^0
0.0
20.0
40.0
60.0
80.0
100.0
120.0
INITIAL ENERGY (EV)

Figure (7b)

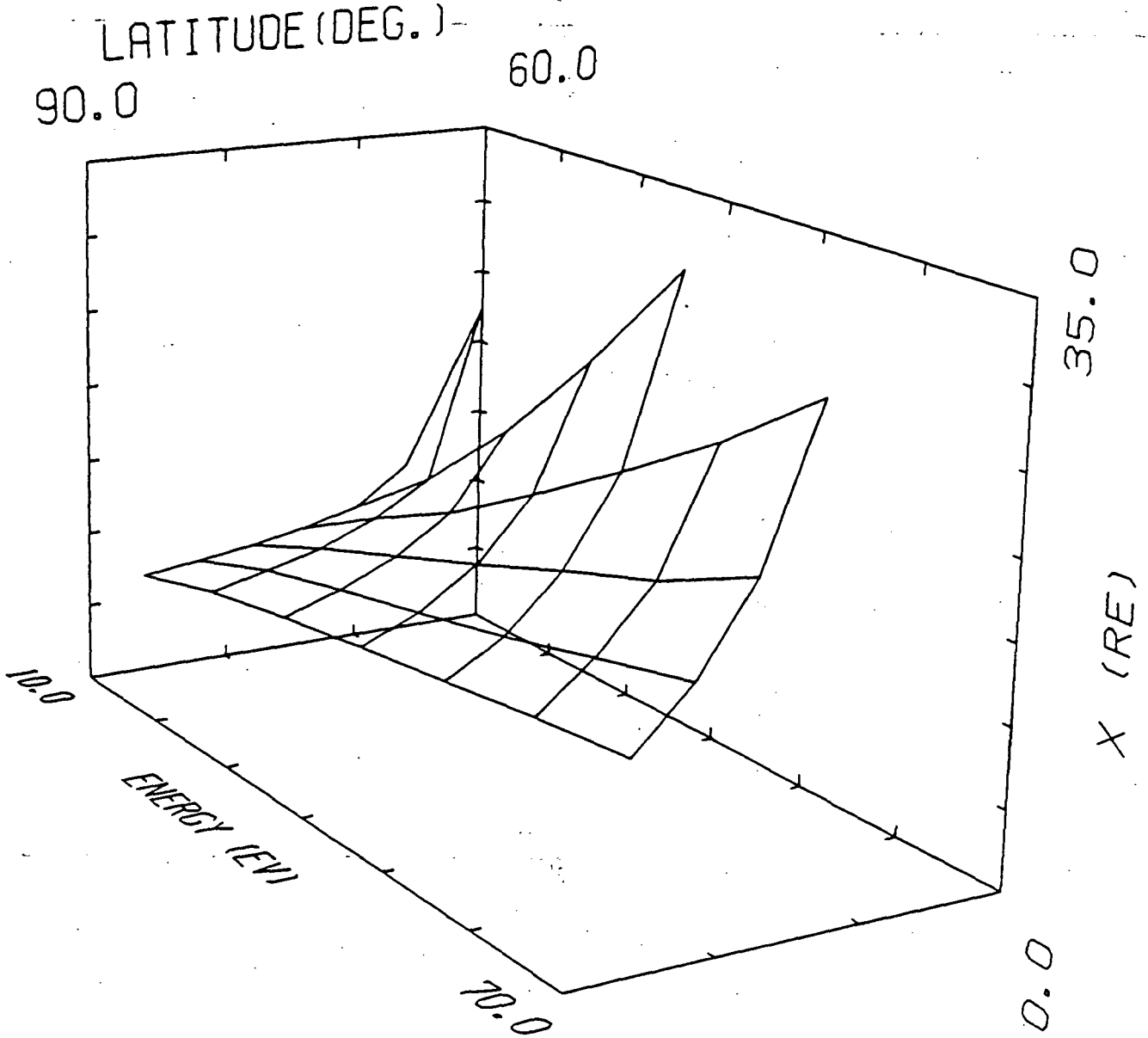

Figure (8a)

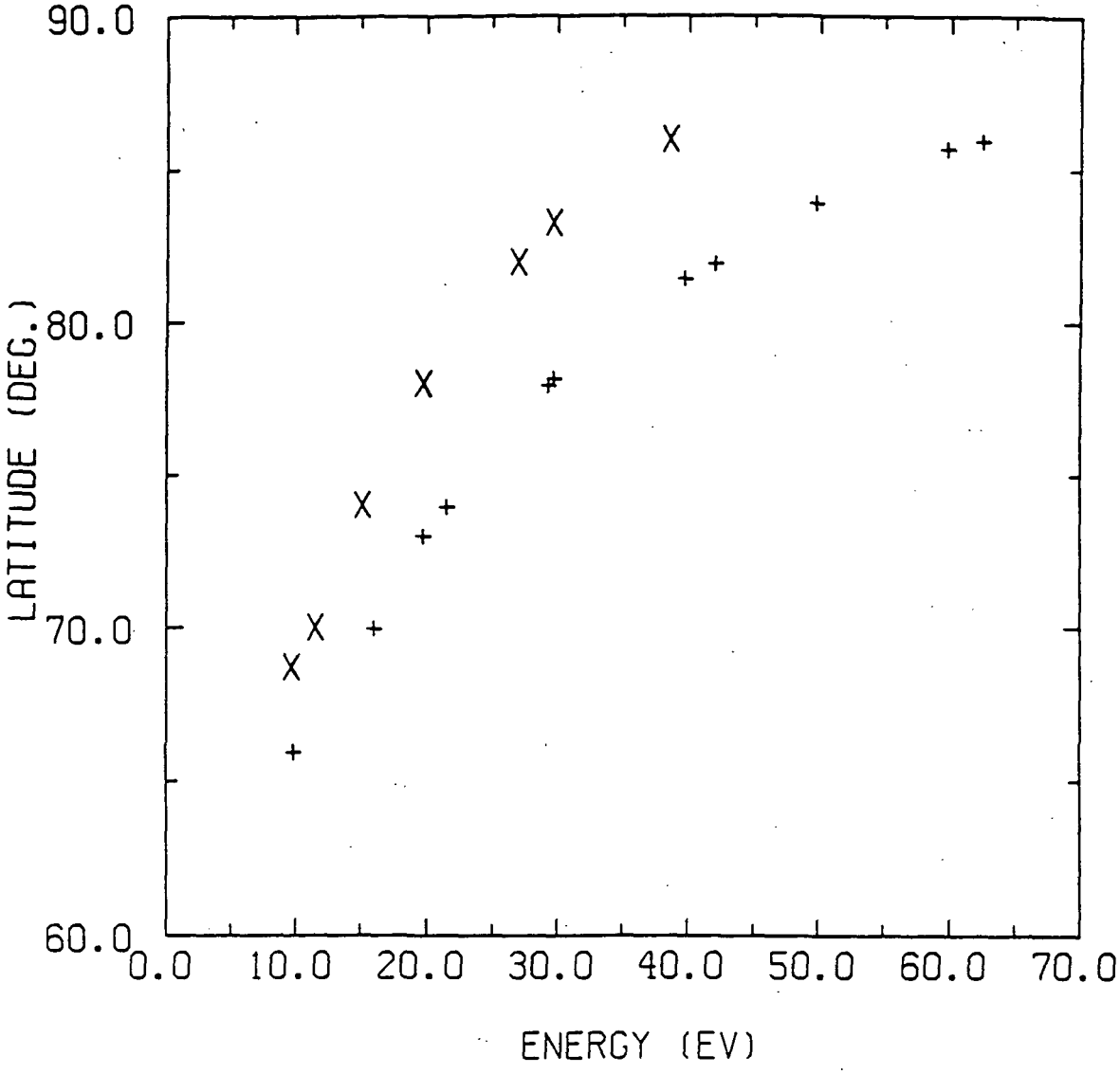
90.0
80.0
70.0
60.0
LATITUDE (DEG.)
0.0
10.0
20.0
30.0
40.0
50.0
60.0
70.0
ENERGY (EV)

Figure (9)